Stress concentrations induced by active and passive reinforcements in a concrete containment building

L. CHARPIN[a], J.-P. MATHIEU[b], T. SOW[c]

a. EDF R&D MMC, laurent.charpin@edf.fr
b. EDF R&D MMC, jean-philippe.mathieu@edf.fr
c. formerly at EDF R&D MMC

Abstract:

EDF studies the behavior of concrete containment buildings since delayed strains of concrete cause the pre-stress to decrease, impairing the containment capacity. This work deals with sub-modelling of a representative part of the VeRCoRs inner wall cylindrical part submitted to delayed strains. First in this paper, a phenomenological constitutive law describing these delayed strains is identified on lab experiments made on VeRCoRs concrete (sealed and drying mass-loss, shrinkage and creep). This law is subsequently used to study the effect of the inhomogeneity of stress and strain fields through the wall due to the presence of passive and active reinforcements. To do so, a representative periodic model of the VeRCoRs wall is studied. First, the effect of the stiffness brought by the steel parts is studied. It is found that they contribute to around 8% of the horizontal and hoop stiffness, and have an even greater impact on radial strains. Second, the stress concentrations around steel bars and pre-stress ducts are observed. Tensions up to 2 MPa can appear after 7 years of creep due to the rigid inclusion effect of the steel bars and ducts. If the transverse reinforcements are taken into account, these tension efforts are largely decreased, confirming the important role of these bars against delamination of pre-stressed concrete walls.

Concrete containment building, VeRCoRs, concrete, creep, pre-stress

1 Introduction

EDF's French nuclear reactors fleet currently under operation is composed of Pressurized Water Reactors. The containment building is the third barrier between radiological hazard and population, hence, ensuring its integrity is crucial in safety demonstration. About half of Concrete Containment Buildings (CCBs) of French nuclear power plants are double-walled. This design has the particularity that the leak-tightness of the containment relies on: (i) the permeability of the 1.2 m post-tensioned inner concrete wall and (ii) a dynamic filtration system in the air gap between the inner and the outer containments. In France, safety is checked by the regulators authority on double walled containment buildings by imposing a maximum permissible leak rate during periodic Integrated Leakage Rate Tests (ILRTs) of the inner wall that occurs about every 10 year. These test are done by submitting the containment to an increase of pressure.

Inner containment buildings leak-tightness mainly relies on the inner wall concrete prestress, so that it has been a matter of interest for engineers to better understand the mechanisms of Presstressed Reinforced Concrete (PRC) prestress loss and its effect on leak-tightness. Both experimental and modelling efforts are undergone to understand and simulate these effects on representative structures [11]. To overcome the difficulty of such experiment to be fully representative, the VeRCoRs mock-up - a 1/3 concrete double-walled containment building - is the most recent and important effort made at EDF to better understand the links between ageing mechanisms (drying, shrinkage, creep, damage) and leak-tightness.

Global simulations of containment buildings ageing are now available to civil engineers [7], but the explicit link between prestress loss and decrease of leak-tightness remains to be clarified. However, regarding the PRC, one can not afford to fully represent the whole complexity in containment simulations. Even when rebars and tendons are explicitly represented in simulations, they are accounted for as simplified structural elements at scales that are not adequate to such studies. Hence, although the great contrast in mechanical properties is generally a key issue it can't be addressed with full structural simulations. The VeRCoRs experiment is an unique opportunity to study realistic ageing conditions on a structure that is also specifically dedicated to experiments. Its inner wall was pre-stressed in 2015 and it will be operated for 7 years onwards.

This study focuses on a Representative Periodic Pattern (RPP) of the regular part of the cylindrical inner wall of VeRCoRs. It discusses the effects of the inhomogeneity of stress and strain fields through the wall due to the presence of passive and active reinforcements in the PRC, following previous works such as [10, 9].

First sections will present the concrete constitutive models and calibration process concerning drying, shrinkage, and creep. In the second part of the paper, the identified constitutive behaviors will be implemented in a RPP model to study the effects of active and passive reinforcements. These effects will mainly be discussed in terms of long term stiffness and prestress loss as well as stress concentrations, since no damage is accounted for and the pressure tests are not taken into account in this preliminary work.

2 Presentation of the constitutive model

This presentation of the constitutive model is inspired from [5].

2.1 Drying model

The drying model used in this study is available in `Code_Aster` under the name `SECHAGE_GRANGER`. It was implemented by [6] from [13]. A non-linear diffusion equation governs the evolution of the water concentration C (L/m^3). It writes $\frac{\partial C}{\partial t} - \mathrm{div}[D(C,T)\mathrm{grad}C] = 0$. In isothermal conditions, the diffusion coefficient simply writes $D(C,T_0) = A\exp(BC)$ [13]. The dependence on the temperature is described by the following equation $D(C,T) = D(C,T_0)\frac{T}{T_0}\exp\left[-\frac{Q}{R}\left(\frac{1}{T}-\frac{1}{T_0}\right)\right]$. The temperatures are expressed in Kelvin. Parameter A governs the kinetics while B governs its dependence on the water concentration. Another important parameter is the boundary condition C^{eq} which is imposed as a fixed water concentration at the boundary. It represents the water concentration of the concrete at the relative humidity of the test room.

2.2 Delayed strains model

The mechanical model was originally developed for EDF R&D by [2]. It was then modified in order to better represent long term basic creep according to [16], and recently implemented in [14] under the name BurgerAgeing through a collaboration between EDF R&D and F. Benboudjema[1]. It is based on an additive decomposition of the strain in four main contributions: elastic strain, drying shrinkage strain, basic creep strain, and dessication creep strain.

Drying shrinkage The drying shrinkage rate is assumed proportional to the water concentration rate, which writes $\dot{\boldsymbol{\varepsilon}}^{shr} = -k^{shr}\dot{C}\mathbf{1}$ where $\mathbf{1}$ is the second order identity tensor and k^{shr} is a parameter to identify.

Elasticity and basic creep The combination of elastic and basic creep strains is formed as a Burgers rheological model (see Figure 1). Elasticity and basic creep are isotropic and hence, the Burgers model is duplicated in deviatoric and spherical chains. For each chain (d relates to deviatoric and s relates to spherical), the strain is composed of elastic strain (ε_s^{el} and $\boldsymbol{\varepsilon}_d^{el}$), reversible basic creep modeled by the Kelvin-Voigt element (ε_s^{rbc} and $\boldsymbol{\varepsilon}_d^{rbc}$) and irreversible basic creep modeled by the Maxwell element by using a viscosity which is not constant in time (ε_s^{ibc} and $\boldsymbol{\varepsilon}_d^{ibc}$): $\boldsymbol{\varepsilon}^{bc} + \boldsymbol{\varepsilon}^{el} = \left(\varepsilon_s^{el} + \varepsilon_s^{rbc} + \varepsilon_s^{ibc}\right)\mathbf{1} + \left(\boldsymbol{\varepsilon}_d^{el} + \boldsymbol{\varepsilon}_d^{rbc} + \boldsymbol{\varepsilon}_d^{ibc}\right)$. For any tensor, the spherical part is computed as $t_s = \operatorname{tr}\boldsymbol{t}/3$ while the deviatoric part is computed as $\boldsymbol{t}_d = \boldsymbol{t} - t_s\mathbf{1}$.

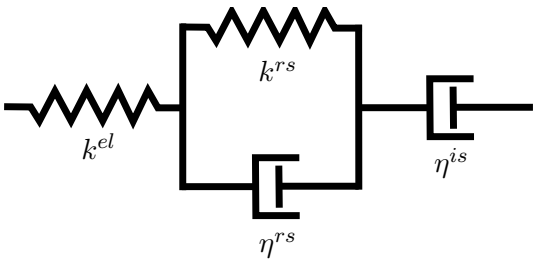

Figure 1: Burgers model (spherical chain)

Figure 2: Drying shrinkage test

The equations related to this Burgers model are now recalled for the spherical chain (the deviatoric can be obtained by replacing s by d and using tensors instead of scalars). The elastic strain is simply proportional to the stress: $\varepsilon_s^{el} = \sigma_s/(3k^{el})$. The basic creep strains are assumed proportional to the water concentration. The reversible basic creep is governed by the equation $\frac{C}{C_0}\sigma_s = k^{rs}\varepsilon_s^{rbc} + \eta^{rs}\dot{\varepsilon}_s^{rbc}$ while the irreversible one follows the equation $\frac{C}{C_0}\sigma_s = \eta^{is}\dot{\varepsilon}_s^{ibc}$ (where C_0 is the initial water concentration)[2].

[1] It is close to the model available in `Code_Aster` under the name `BETON_BURGER_FP`, but the main difference is that the various dependences on moisture are taken into account using the water concentration instead of relative humidity.

[2] Note that coefficients relative to the creep part of the Burgers model where not defined rigorously equivalently to elastic

The viscosity of the irreversible contribution is assumed variable in time and writes $\eta^{is} = \eta_0^{is} t^{\alpha}$, where the time t used is the age of the sample [8]. This feature introduces some kind of ageing and irreversibility in the model and that the same time ensures that the very long term (meaning for $t \gg \eta^{rs}/k^{rs}$ and $t \gg \eta^{rd}/k^{rd}$) creep is logarithmic if $\alpha = 1$, or its rate is a power of time otherwise.

Therefore, a large number of parameters is introduced: k^{el}, μ^{el}, k^{rs}, k^{rd}, η^{rs}, η^{rd}, η_0^{is}, η_0^{id}, α. However, assuming that the basic creep Poisson's ratio is constant and equal to the elastic one, the number of independent parameters can be reduced. The elastic Poisson's ratio writes : $\nu^{el} = (3k^{el} - 2\mu^{el})/(2(3k^{el} + \mu^{el}))$. Equivalently, $k^{el}/\mu^{el} = (2(1+\nu^{el}))/(3(1-2\nu^{el}))$. Therefore, the basic creep parameters can be related through the equations $\eta^{is}/\eta^{id} = \eta^{rs}/\eta^{rd} = k^{rs}/k^{rd} = (1+\nu^{el})/(1-2\nu^{el})$.

Desiccation creep Finally, the desiccation creep is computed according to a modified version of a law called Bažant's law, relating the excess of strain rate during drying to the rate of change of the water concentration [1]. The modifications are related to the multiaxial behavior of concrete and are detailed in [5]. The desiccation creep model was modified so as to have the same Poisson's ratio as elasticity and basic creep. This modification was motivated by a study of the experimental results showing that both basic and drying creep Poisson's ratio were almost constant [3].

The dessication creep strain is composed of spherical and deviatoric parts: $\dot{\boldsymbol{\varepsilon}}^{fd} = \dot{\boldsymbol{\varepsilon}}_d^{fd} + \dot{\varepsilon}_s^{fd}\mathbf{1}$. The spherical strain evolves according to the equation $\dot{\varepsilon}_s^{fd} = \frac{1}{\eta^{fds}} \frac{\dot{C}}{C_0} \sigma_s$. The deviatoric strains follows a similar equation. Since the Poisson's ratio for dessication creep is intended to be constant and equal to the elastic one, the two dessication creep parameters are related by the equation $\eta^{fds}/\eta^{fdd} = (1+\nu^{el})/(1-2\nu^{el})$.

As shown in [5], this modification has largely improved the ability of the model to reproduce dessication creep strains measured in biaxial tests performed at EDF CEIDRE TEGG.

2.3 Parasite mass-loss on sealed samples

The instrumented sealed samples have lost water to various extents depending on their shape (cylindrical, prismatic) and their instrumentation. Concerning the prismatic samples, it is assumed that the parasite mass-loss undergone by the sealed creep and sealed shrinkage samples is similar. This mass-loss is parametrized using the expression $\frac{\Delta m}{m}(t) = \gamma\sqrt{t}\mathrm{e}^{-\frac{t}{\tau}} + \beta\left(1 - \mathrm{e}^{-\frac{t}{\tau}}\right)$ which is an empirical equation which gave satisfactory results.

3 Model identification

The model parameters have been identified using drying, shrinkage and creep tests performed at EDF CEIDRE TEGG. A detailed description of a similar test campaign on a different concrete formula is given in [4, 3]. The actual test campaign is composed of 6 tests performed on 16×100 (cm×cm) cylindrical samples:

- sealed mass-loss test: aims at verifying that the sealing procedure (4 layers of auto-adhesive aluminum foil plus a sprayed varnish) is efficient. This sample is not instrumented which is a limiting factor regarding its representativity with the sealed creep and sealed shrinkage samples.

ones. To do so, one would have to replace k^{rs} by $3k^{rs}$, η^{rs} by $3\eta^{rs}$, k^{rd} by $2k^{rd}$ and so forth in the equations. This is of little practical consequences but needs to be mentioned to avoid confusion.

- drying mass-loss: this sample is allowed to dry due to exposure to the atmosphere of the test room which is regulated in temperature (20±1°C) and relative humidity (50±5 % in theory, but in practice 50±10 %).
- sealed shrinkage: this sample is sealed similarly to the sealed mass-loss sample, and is also instrumented so as to measure its shrinkage. As can be seen on figure 2, the measurement basis is 50 cm long, in the center of the sample. Only one LVDT sensor is used, it measures a mechanical average of displacements differences taken on 3 lines 120 degre. The radial strain is also measured using 3 LVDT sensors held by an invar ring. The LVDT points to a glass window glued directly on concrete. As it will be discussed later (and is also discussed in [4]), these penetrations through the aluminum foils induce water loss.
- drying shrinkage: this sample is allowed to dry and is instrumented in the same manner as the sealed shrinkage sample.
- sealed creep: this sample is placed in the same conditions (atmosphere and instrumentation) as the sealed shrinkage one. In addition to that, it is loaded to an initial stress of approximately 12 MPa. Due to limitations of the pressure accumulator used to maintain the pressure during creep, stresses can decrease of roughly 10 %.
- drying creep: this sample is in the same conditions as the drying shrinkage one, and is loaded identically to the sealed creep sample.

3.1 Drying model

First, the drying mass-loss sample has been modeled by finite elements as 2D axi-symmetric with one element in the axial direction. A linear mesh has been used. The Granger drying model has been used, and parameters A, B and C_{eq} have been identified, yielding the best fit shown on figure 3.

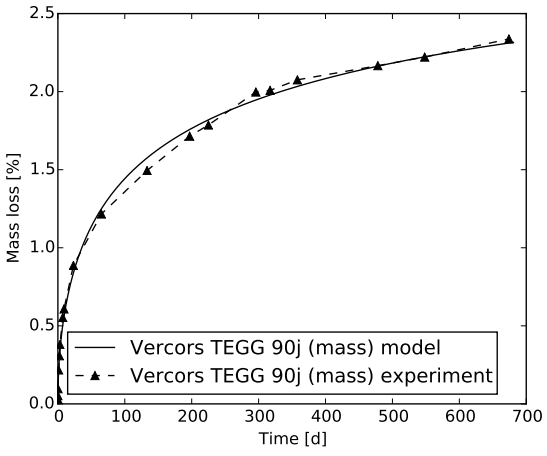

Figure 3: Drying mass-loss

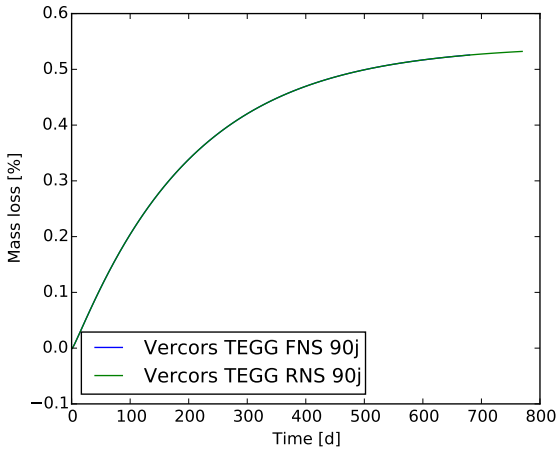

Figure 4: Parasite mass-loss for sealed tests

The initial water concentration was assumed to be $C_0 = 148.72$ L/m^3 according to porosity and saturation measurements performed on concrete samples of the same batch. As proposed by Granger, the activation energy of the Arrhenius term is set to the value $Q/R = 4700$ K. The reference temperature is

taken as $T_0 = 15°C$, and the test temperature is $T = 20°C$. The density of concrete used for calculations of the relative mass loss is $\rho = 2357$ kg/m^3.

The parameters were identified to the values shown in table 1. This set of parameters has been used to

Table 1: Drying model parameters

parameter	A	B	C^{eq}
unit	m^2/s	-	m^2/s
final value	7.48 10^{-15}	0.0766	76.97

simulate the drying of other samples of the same concrete (including samples of different sizes), which improved the confidence in this set of parameters.

3.2 Mechanical model

Second, the mechanical model was calibrated against the creep and shrinkage experimental data. The data used was 420 days of drying creep, sealed creep, and drying shrinkage and also 510 days of sealed shrinkage. All the mechanical model parameters as well as the parasite mass-loss model were calibrated at once, assuming that the same parasite mass-loss occurred in the sealed creep and sealed shrinkage tests. While the initial stress imposed to the creep samples is 12 MPa (i.e. 240 kN on 16 cm diameter samples), the force decreases due to creep and shrinkage of concrete. When the decrease of the force reaches 10 %, it is manually brought back to its initial value. This has been performed after 400 days of creep tests on both creep samples. However, since the impact of this reloading on the strain curves is limited, the load was assumed to be constant.

The parameters of the model were identified to the values shown in tables 2 and 3.

Table 2: Parameters of the mechanical model

parameter	E	ν	k^{rd}	η^{id}	η^{rd}	α	η^{fdd}	k^{shr}
unit	Pa	-	Pa	Pa.s	Pa.s	-	Pa.s	m^3/kg
final value	28.4 10^9	0.268	1.46 10^{10}	7.14 10^{14}	4.38 10^{18}	1.19	7.18 10^9	1.00 10^{-5}

Table 3: Parasite mass-loss parameters

parameter	τ	β	γ
unit	s	kg/m^3	kg/m^3/s$^{1/2}$
final value	1.64 10^7	8.61 10^{-2}	-1.71 10^{-6}

While the identification has been performed using 420 days of data for most tests, the comparison of the simulation and experiment is performed using 770 days of data for sealed shrinkage and 680 days for the other tests, in order to test the extrapolation capabilities of the mechanical model (note that the drying model was identified on 680 days of data directly).

The identified parasite mass-loss is shown on figure 4. It is not negligible compared to the drying mass-loss, which explains the difficulties experienced when trying to simulate the sealed tests without assuming the existence of a parasite mass-loss. The creep strains are shown on figures 5 and 6. As is frequently done when presenting creep and shrinkage test results, contractions are shown as positive

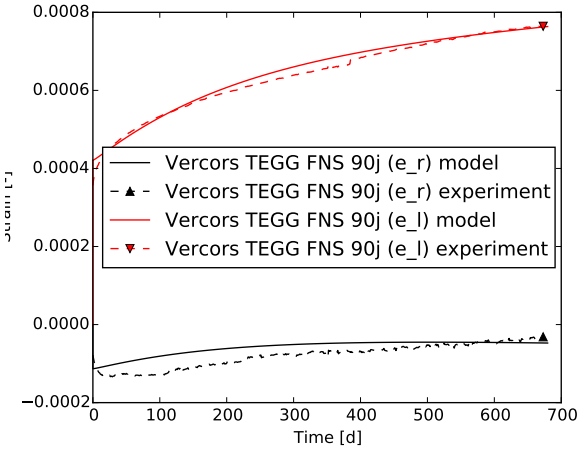

Figure 5: Sealed creep

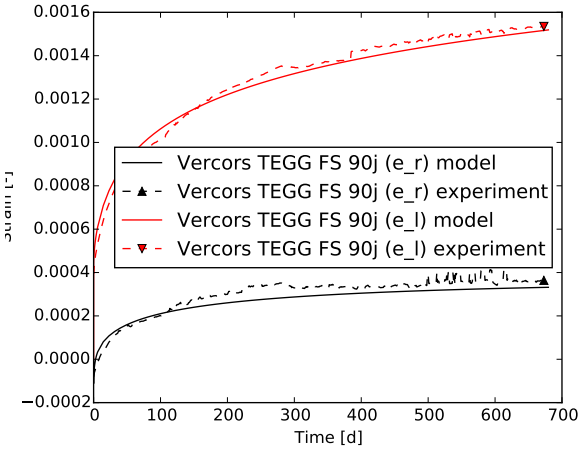

Figure 6: Drying creep

strains. Strains are well reproduced for both tests in both directions. Note that the confidence in the radial strain of the sealed creep test is less than for other tests due to its sensitivity to leaks and to the presence of the glass window glued directly on the sample. The shrinkage strains are shown on figures 7

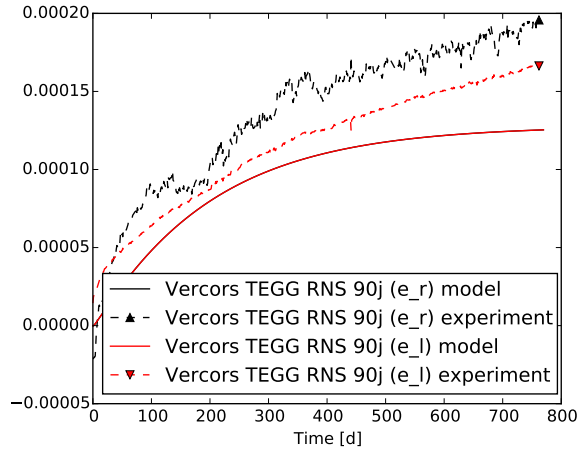

Figure 7: Sealed shrinkage

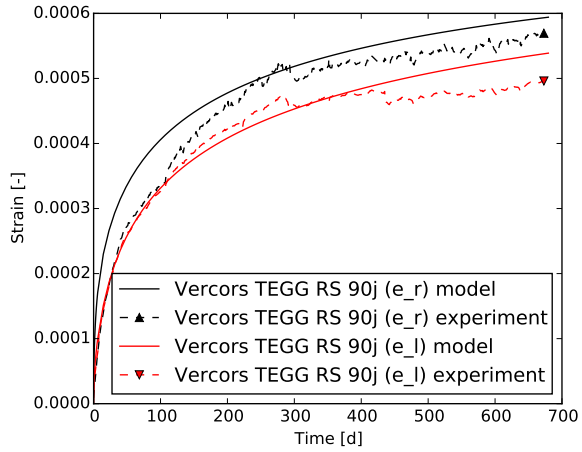

Figure 8: Drying shrinkage

and 8. The strains are well captured including the anisotropy of drying skrinkage strains. Again, the radial strain in the sealed shrinkage test is probably less accurately measured than other strains. Note that no model for autogenous shrinkage was used, which can probably explain why the strain rate at the beginning of the sealed shrinkage test in the axial direction is not well captured. A way of dealing with this would be to add another term to the parasite mass-loss, with the aim to represent auto-dessication.

4 Representative periodic part of VeRCoRs

4.1 Geometry

The focus will be placed on the VeRCoRs mock-up which is a 1/3 mock-up representative of double-wall French Prestressed Reinforced Concrete Containment Building (PRCCBs). To analyze the impact of the rebars and also of the prestress ducts on the overall stiffness of a PRCCB, a RPP of the inner concrete

wall has been identified and modeled by Finite Elements. It is representative of the cylindrical wall in parts where there are no singularities (e.g. access hatch, pipings, see figure 9). In such parts, the position of prestress ducts and rebars, including radial hooked tie bar, is well-defined and periodic. The pattern dimensions are a radial thickness of 40 cm comparable to VeRCoRs inner wall, and two others dimensions of roughly 15 cm. The reinforcement bars, are represented and meshed explicitly, as well as the pre-stress ducts filled with tendons (accounted for as cylinders of equivalent section to real cables ones) encompassed in grouting cement (figure 10).

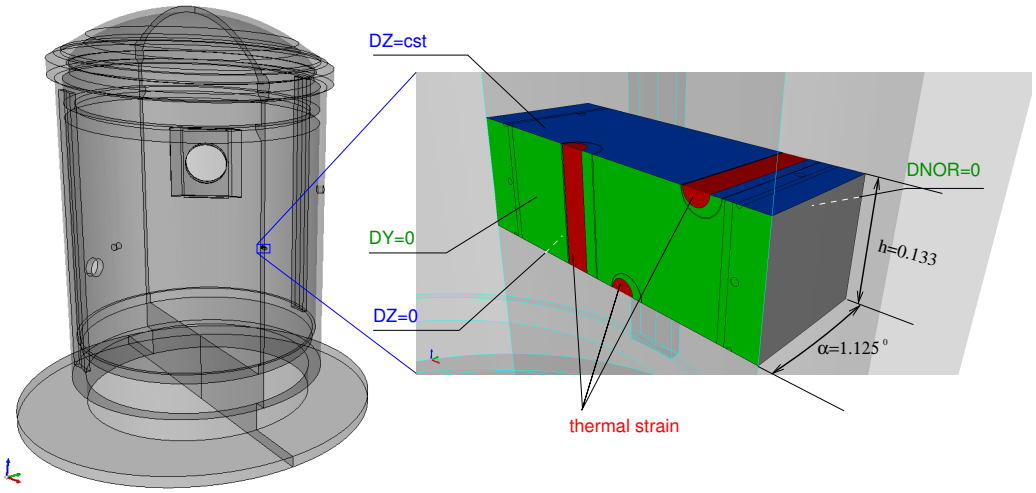

Figure 9: The representative periodic pattern

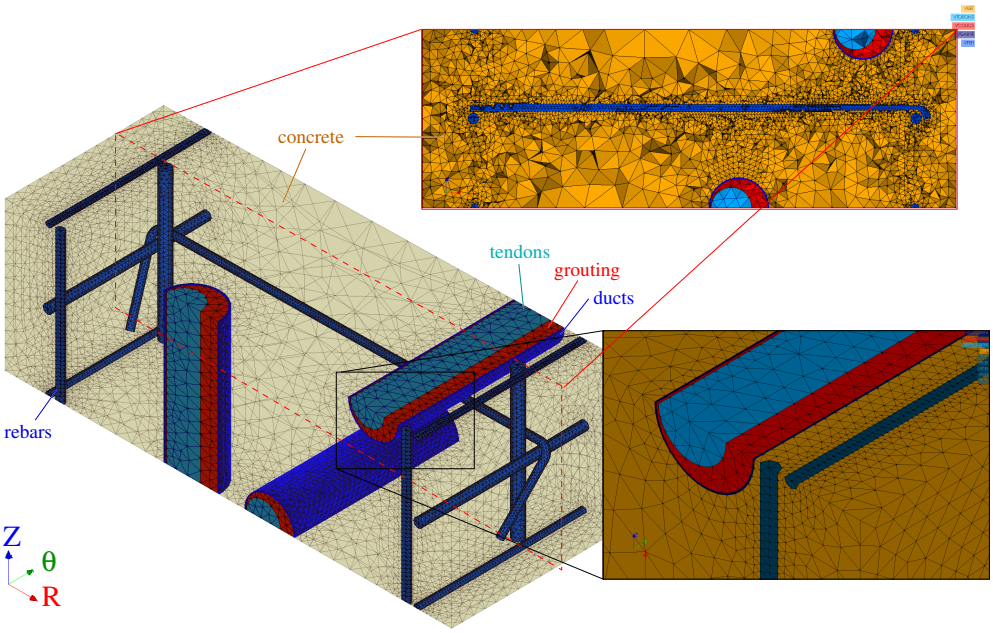

Figure 10: Finite element mesh used for mechanical computations. Details of structural elements are highlighted

Two cases will be studied on a mechanical point of view:

- in the “concrete+steel” calculus, rebars and ducts are made of steel as in the real RPP.

- in the “all concrete” calculus, rebars ans ducts steel elastic constitutive law was replaced by the same material as concrete.

The idea is to study how the rebars and ducts influence the global behavior as well as local stress concentrations so as to determine the best way to take them into account in full CBB simulations where their representation can reach different levels of complexity [9].

4.2 Comments on the modelling

In this preliminary study, comments are made on the cracking risk by analyzing stress concentrations after the prestress. Many points are left aside. First of all, cracking at early-age is not studied. It would require computations of a detailed model of the gusset (a part of the CCB which connects the wall to the raft and is prone to thermal cracking at early age) as well as a knowledge of the tension creep and fracture properties of the concrete used. This work is beyond the scope of the present study.

Instead, it is proposed here to assume that the RPP is stress-free before the beginning of prestress, in order to study the stress concentration due to prestress and drying. Cracking is not modelled, and the interfaces between steel and concrete parts are assumed to be perfect. As mentioned in the sequel, more refined studies dealing with the computation of damage in concrete are planed in the future.

4.3 Global analysis: drying

First, the drying of the RPP is modeled using the same drying model as earlier and the parameters identified using the lab experiments. The modelling result will be used as an entry to subsequent mechanical modelling.

During VeRCoRs mock-up construction, the concrete of the inner wall was kept continuously wet until the prestressing phase. This phase occurred between 1 month (dome) and 1 year (base part) of age of concrete. This can be considered consistent with the age of 90 days used in the lab experiments for both drying, creep and shrinkage. In this first approach, the real and detailled temperature and humidity evolutions around the VeRCoRs mock-up were not used. However, developments are under progress in this direction so as to compare results with field measurements.

The saturation profiles obtained assuming that the conditions are T=20 °C and RH=50 % are plotted in figure 11. The concrete which is initially saturated reaches around 95 % saturation at the center of the wall after 6 months, and then 90 %, 80 % and 75 % after 1, 4 and 7 years after the beginning of drying. Water content measurements are currently being performed and analyzed on VeRCoRS [15]. They shall be used to validate the drying model in future work.

4.4 Mechanical boundary conditions and loadings

Pseudo-periodic boundary conditions were applied to the RPP and are described in figure 9. `DNOR` stands for normal displacements according to the surface. Prestress was applied by using a "virtual" thermoelastic loading in the tendons: their thermal expansion coefficients have been considered transverse isotropic according to their longitudinal direction, in order to impose a longitudinal shortening. Grouting elastic modulus was taken as one hundredth of its final value during the elastic prestress tensionning phase, and raised to its final value at the beginning of the creep calculation; constitutive laws were applied as follow:

- concrete: mechanical constitutive law as calibrated in section 3.2

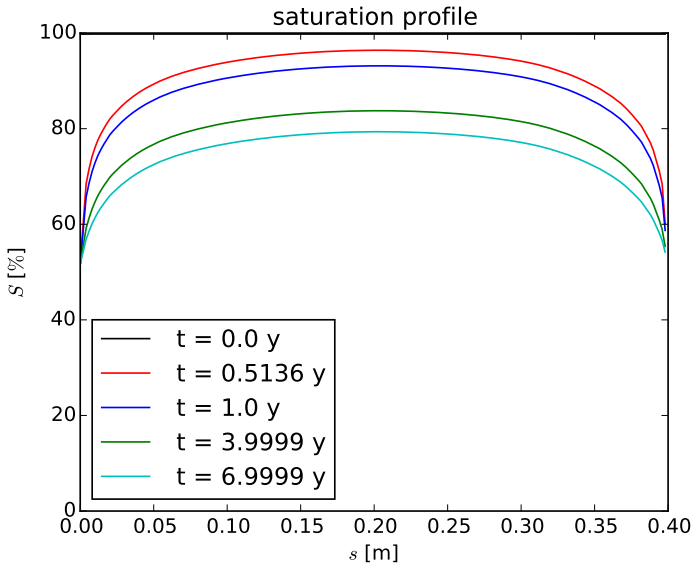

Figure 11: Evolution of the saturation across the RPP thickness in time.

- grouting mortar: isotropic elastic; $E = 28.4$ GPa; $\nu = 0.268$ ($E = .284$ GPa during prestress phase)
- rebars, ducts and tendons: isotropic elastic $E = 197$ GPa; $\nu = 0.3$ (only for "concrete+steel" calculus)

The interface between different materials (concrete, rebars, prestress ducts, grouting morta) is assumed to be perfect.

The use of thermoelasticity in tendons is a simple way to apply prestress, but its representativeness is questionable. It also requires adjustments to obtain the good level of prestress in the structure in both vertical (Z) and hoop (θ) directions, and has the drawback that it can only be used if no temperature evolution is taken into account (which is the case in this preliminary modelling).

The aim of the following part is to show the impact of presence of the ducts and rebars on the mechanical behavior of the PRCCB both from a global and local point of view.

4.5 Global analysis: delayed strains

Using this saturation repartition, the mechanical response under the prestress imposed according to previous section 4.4 is computed. The magnitude of the thermal contraction for each direction of the tendons (vertical and hoop) was adjusted so as to achieve the correct amount of prestress on the full volume of the model except the tendons: 12 MPa in the hoop direction and 8.5 MPa in the vertical one. Once the prestress is finished, the tendons behave elastically.

The prestress hence decreases due to concrete creep and shrinkage as can be seen on figures 12 and 13.

Both "concrete+steel" and "all concrete" case are studied. In both cases, prestress slowly decreases by 1 to 2 MPa in the 7 years of VeRCoRs life span. As mentioned earlier, the reason for this decrease is the delayed strains experienced by concrete itself. These strains can be examined globally using averages on the full volume except tendons, as done earlier for the stress. Vertical (figure 14) and hoop (figure 15) strains show large variations due to creep and skrinkage.

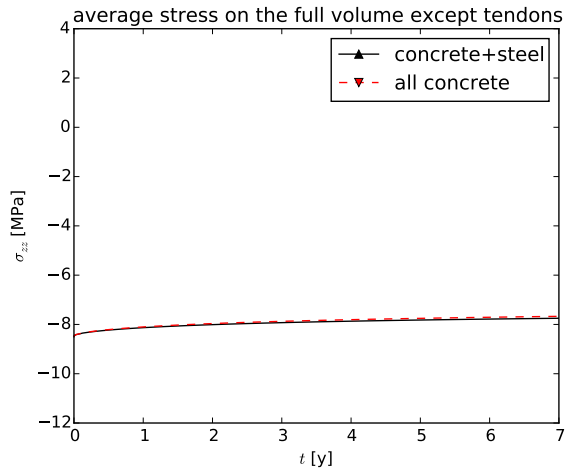

Figure 12: Vertical average stress

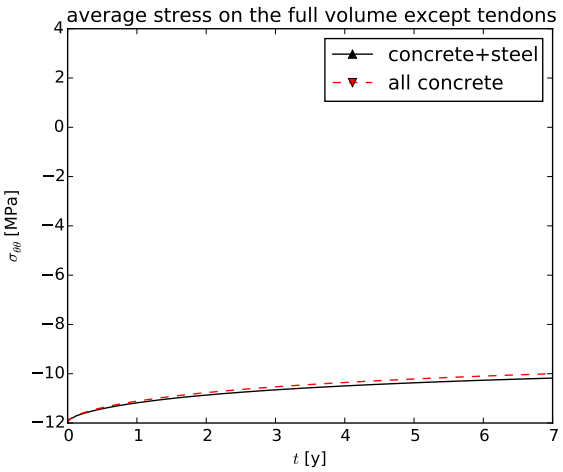

Figure 13: Horizontal average stress

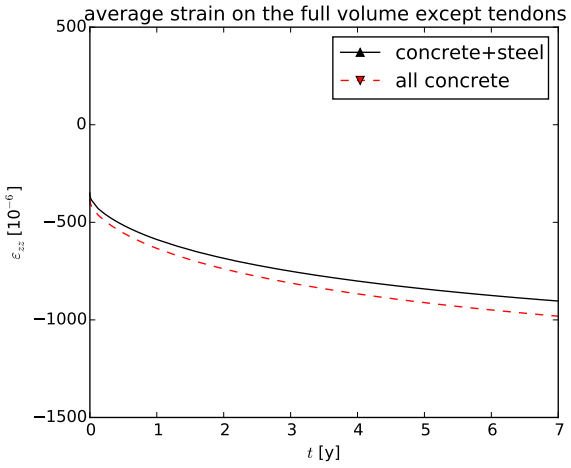

Figure 14: Vertical average strain

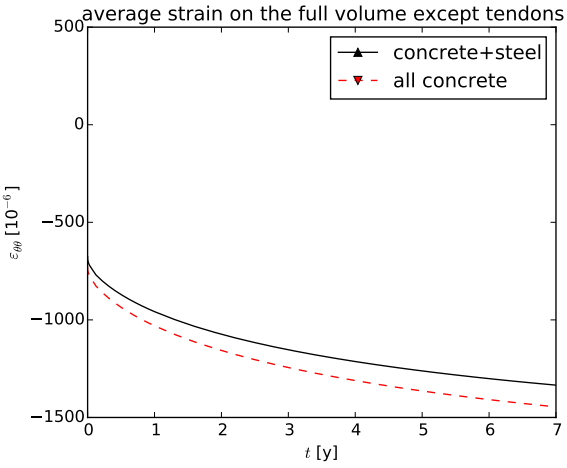

Figure 15: Horizontal average train

As expected, strains are larger in the “all concrete” case at loading and even more at later ages. The “concrete+steel” case is 7 to 8 % stiffer during the entire time range. This phenomenon is even more pronounced in the wall thickness direction which is not loaded but deforms under the opposite effects of drying shrinkage on the one hand, and creep Poisson’s effect on the other hand. This is shown in an absolute way on figure 16 and in terms of relative difference on figure 17.

In both computations, the effect of shrinkage is larger than that of creep Poisson’s effect, inducing a global decrease of the wall thickness after loading. The difference between the two computations increase over time and reach 20 % after 7 years. This effect is probably mainly due to the very important role of the hooked tie bars which are in put in traction at loading and hence, limit the creep Poisson’s effect. To verify this assertion, a computation removing only these rebars shall be performed in the future.

4.6 Local analysis

The advantage of performing detailed computations is the ability to access to the local values of stresses and strains. This gives an idea of the risks of cracking experienced by the concrete wall. Even in the

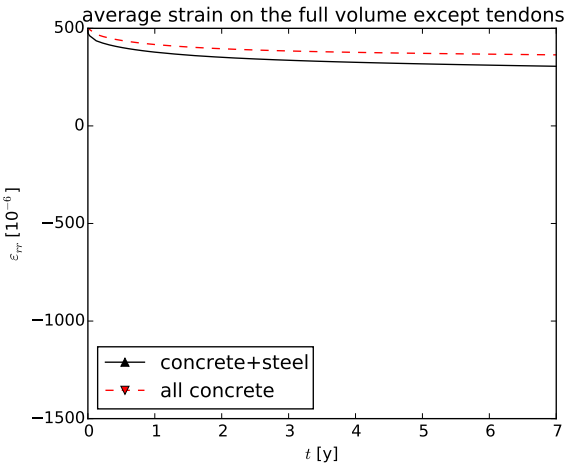

Figure 16: Radial average strain

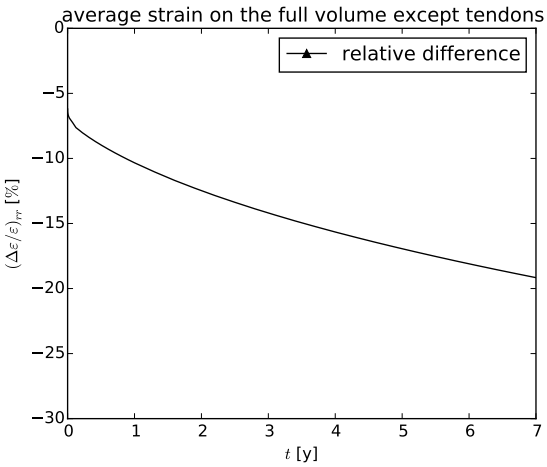

Figure 17: Relative difference of radial strains

context of the present simulations where no damage or cracking model is used, the cracking risk is commented. Further developments including damage as in [9, 12] will be attempted in the future.

4.6.1 Drying effects

Cracking can occur due to moisture gradients: drying promotes shrinkage and creep close to the faces of the wall. Hence, the vertical stress varies largely in the thickness of the wall as seen on figure 18 along a line which goes through the wall thickness as far as possible from any rebar or duct. At the beginning of drying, the surface of concrete even experiences tractions which could induce cracking and surely would if the pre-stress was removed, or during IRLTs during which CBBs are inflated up to a relative pressure of 4.25 MPa. However, one can notice that only the concrete cover seems concerned by this effect. To gain more insight on this phenomenon, IRLTs will be simulated in the next versions of this calculus. The tractions experienced by the concrete cover vanish with the flattening of the saturation profile over time.

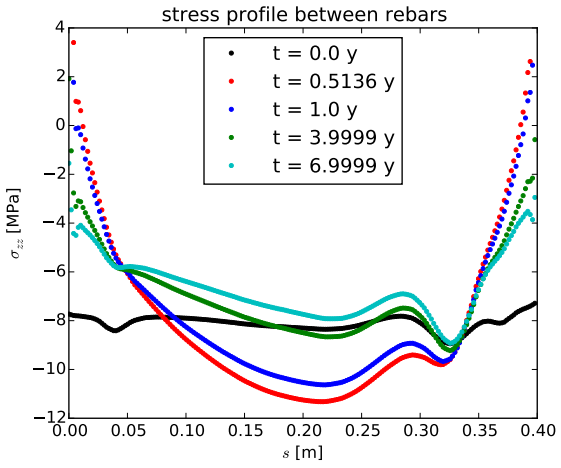

Figure 18: Vertical stress profile across the wall

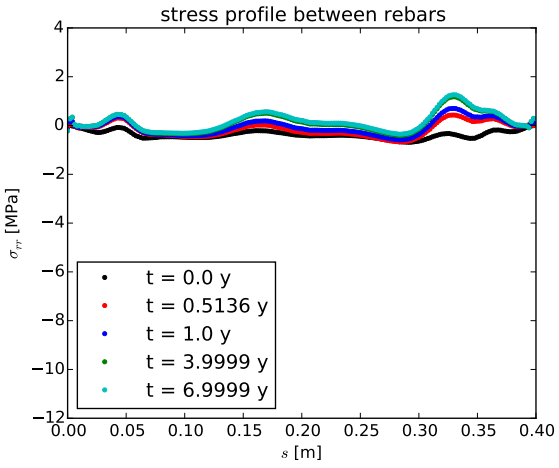

Figure 19: Radial stress profile across the wall

The radial stress profile (figure 19) also exhibits tractions which reach 1.5 MPa at 7 years. These level

of tractions are low enough to avoid any effect like delamination of the cover of the concrete wall in the plane of the outer rebars.

4.6.2 Heterogeneity effects

Stress concentrations are also induced by the stiffness contrast between metallic parts and concrete. As an illustration, the radial stress profile along a vertical line crossing the outer hoop rebars is plotted on figure 20.

While consequently to the prestress loading only moderate tractions are found in the RPP, the creep in concrete induces stress concentrations close to the rebars after 7 years of VeRCoRs ageing. The tractions reach up to 3 MPa, which is close to the strength in tension of the VeRCoRs concrete which is equal to 5 MPa (measured by a brazilian test). However, conversely to the strain concentrations mentioned in paragraph 4.6.1, these strain concentration are not expected to increase during IRLTs.

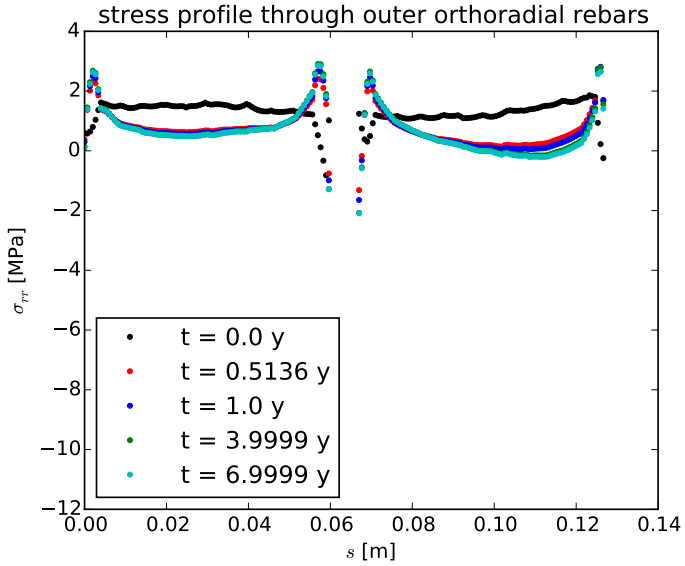

Figure 20: Radial stress profile in concrete across outer hoop rebars. The abscissa s corresponds to coordinate z.

More surprisingly, tension stress concentrations are also found between rebars in the loaded directions after 7 years, as can be seen on figure 21. These tensions reach 1.5 MPa and would increase during the IRLT, probably inducing damage. They are related to an interaction between the external hoop prestress duct and rebars. Although leak-tightness mainly rely on the volume of concrete between the duct layers, this type of cracking understanding is probably important to consider properly in order to better predict leakage evolution of PRCBBs.

Another type of stress concentration is that related to the vertical ducts as seen after 7 years of prestress on figure 22. Tension stresses are observed due to the inclusion effect of the ducts. However, these stresses should vanish during the IRLT. Therefore the question is whether they have to be considered as less critical to the leak-tightness of the PRCBB than those shown on figure 21.

Importantly, no tension stress concentrations are induced close to the hooked tie bars: These are the only steel elements going through the wall. Indeed if the transport of air was promoted due to damage along

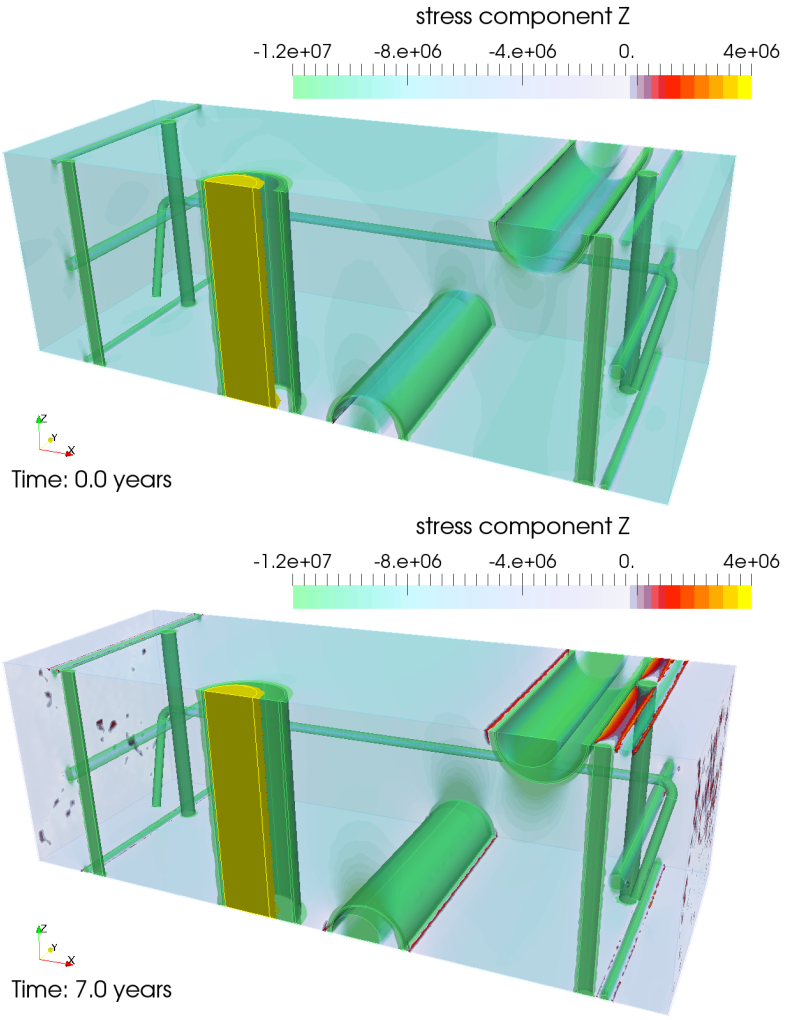

Figure 21: Vertical stress concentrations after prestress and after 7 years

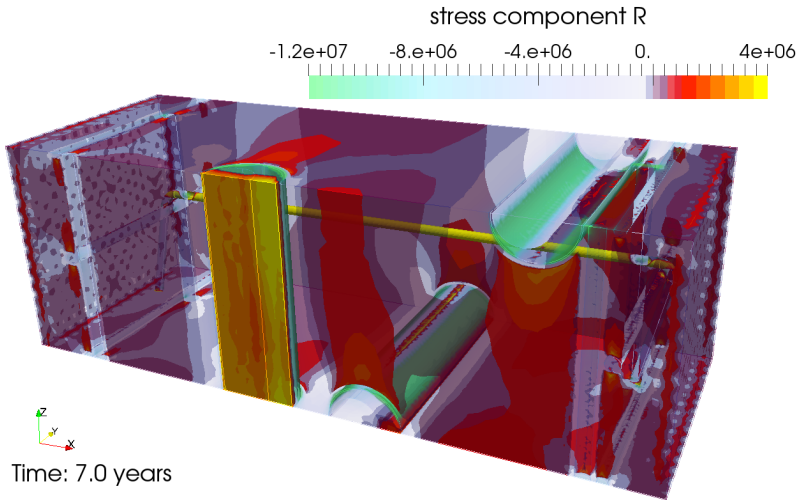

Figure 22: Radial stress concentration after 7 years

these bars, the impact of the leak-tightness of the structure would probably be very large, which is not observed on PRCBBs.

4.7 Discussion

This local analysis is a preliminary work that confirms that the damage can occur in the concrete cover and in the vicinity of prestress duct, but it does not exhibit any risk of extent of through wall damage.

Several limitations of this simulation work are recalled in the following:

- Constitutive laws do not include any damage;
- Realistic VeRCoRs temperature and humidity profiles were not accounted for;
- ILRTs were not modeled in this preliminary work;
- Effect of the radial hooked tie bars could have been studied specifically, as they are generally not accounted for in modelling (on contrary to the other rebars that are generally accounted for by mixed or specific structural elements).

This local analysis will thus be extended by improving these aspects which should make the comparison with experimental data acquired on VeRCoRs possible. Once validated, further work on this modelling will also include its use in order to improve the understanding of through wall leaks of PRCCBs.

The insight gained on the global effect also gives interesting perspectives to take these effects into account in full structure computations: a transverse isotropic constitutive law could be used for concrete in order to mimic the stiffness brought by the rebars without having to represent them explicitly. However, this approach would not be accurate for more complex loading cases not studied in this paper such as bending (e.g. at the bottom of the wall, close to the base), and would not be able to take into account local effects either.

5 Conclusion

In this paper, a discussion about the influence of the rebars and prestress duct on the global and local behavior of PRCCBs is proposed. To do so, a RPP of the VeRCoRs mock-up cylindrical part is used. The parameters of the constitutive model are identified using laboratory tests of roughly 400 days length.

The computations of the delayed strains of the RPP under prestress exhibits a large influence of the rebars and prestress ducts, both from a global and local perspective. The insight gained on the global effect provides perspectives to take these effects into account in full structure computations. However, this approach also leads to limits in representativity. Therefore, in parallel of homogenized approaches for the material constitutive behavior in full structure computations, studies on refined model as presented in this paper must be pursued and refined, both to improve the global models by comparing them to the results of such approaches and to achieve a better understanding of the leak phenomena on a more local scale.

References

[1] Z.P. Bažant and J.C. Chern. Concrete creep at variable humidity: constitutive law and mechanism. *Materials and structures*, 18(1):1–20, 1985. *p. 4*

[2] F. Benboudjema. *Modélisation des déformations différées du béton sous sollicitations biaxiales. Application aux enceintes de confinement de bâtiments réacteurs des centrales nucléaires*. PhD thesis, Université de Marne la Vallée, 2002. *p. 3*

[3] L. Charpin, Y. Le Pape, E. Coustabeau, B. Masson, and J. Montalvo. EDF study of 10-years concrete creep under unidirectional and biaxial loading: evolution of Poisson coefficient under sealed and unsealed conditions. In *CONCREEP 10, Vienna, Austria*. 2015. p. 4

[4] L. Charpin, Y. Le Pape, E. Coustabeau, B. Masson, J. Montalvo, N. Reviron, A. Courtois, J. Sanahuja, E. Toppani, C. Le Bellego, and G. Heinfling. EDF Study of 10-Years Concrete Creep under Unidirectional and Biaxial Loading. *To be submitted*. p. 4 and 5

[5] L. Charpin, T. Sow, X. d'Estève de Pradel, F. Hamon, and J.-P. Mathieu. Numerical simulation of 12 years long biaxial creep tests. Efficiency of assuming a constant Poisson's ratio. In *6th BIOT conference, Champs sur Marne, France*. 2017. p. 2 and 4

[6] L. Granger. *Comportement différé du béton dans les enceintes de centrales nucléaires : analyse et modélisation*. PhD thesis, Laboratoire Central des Ponts et Chaussées, France, 1995. p. 2

[7] J. Haelewyn, P. Semete, J.-P. Mathieu, F. Escoffier, S. Michel-Ponnelle, F. Hamon, and E. Buchoud. A numerical clone for VeRCoRs mock-up. In *CFM 2017, Lille, France*. 2017. p. 2

[8] A. Hilaire. *Etude des déformations différées des bétons en compression et en traction, du jeune au long terme: application aux enceintes de confinement*. PhD thesis, Cachan, Ecole normale supérieure, 2014. p. 4

[9] L. Jason, S. Ghavamian, and A. Courtois. Truss vs solid modeling of tendons in prestressed concrete structures: Consequences on mechanical capacity of a representative structural volume. *Engineering Structures*, 32(6):1779–1790, 2010. p. 2, 9, and 12

[10] L. Jason, S. Ghavamian, A. Courtois, and L. Illie. Simulation of the prestress in a representative structural volume of a french 1450 mwe containment building. In *19th international conference on structural mechanics in reactor technology (SMIRT), Toronto*, volume 8, 2007. p. 2

[11] L. Jason and B. Masson. Comparison between continuous and localized methods to evaluate the flow rate through containment concrete structures. *Nuclear Engineering and Design*, 277:146–153, 2014. p. 2

[12] A. Llau, L. Jason, F. Dufour, and J. Baroth. Modelling strategies of prestressing tendons and reinforcement bars in concrete structures. In *VII European Congress on Computational Methods in Applied Sciences and Engineering*, 2016. p. 12

[13] R Mensi, P Acker, and A Attolou. Séchage du béton: analyse et modélisation. *Materials and structures*, 21(1):3–12, 1988. p. 2

[14] MFront. http://tfel.sourceforge.net/, 2016. p. 3

[15] E. Oukhemanou, S. Desforges, E. Buchoud, and A. Courtois. VeRCoRs Mock-Up: Comprehensive Monitoring System for Reduced Scale Containment Model. In *TINCE 2016, Paris, France*. 2016. p. 9

[16] A. Sellier and L. Buffo-Lacarrière. Vers une modélisation simple et unifiée du fluage propre, du retrait et du fluage en dessiccation du béton. *European Journal of Environmental and Civil Engineering*, 13(10):1161–1182, 2009. p. 3